© 2015

Crystallization Behavior of Amorphous Ti$_{51.1}$Cu$_{38.9}$Ni$_{10.0}$ Alloy

Marcio Andreato Batista Mendes[a]*, Claudio Shyinti Kiminami[b], Walter José Botta Filho[b],

Claudemiro Bolfarini[b], Marcelo Falcão de Oliveira[c], Michael Joseph Kaufman[d]

[a]*Departamento de Engenharia de Materiais, Universidade Federal Tecnológica do Paraná – UTFPR,*
Av. dos Pioneiros, 3131, CEP 86036-370, Londrina, PR, Brazil
[b]*Departamento de Materiais, Universidade Federal de São Carlos – UFSCar, São Carlos, SP, Brazil*
[c]*Departamento de Engenharia de Materiais, Aeronáutica e Automobilística,*
Universidade de São Paulo – USP, São Carlos, SP, Brazil
[d]*Departament of Metallurgical and Materials Engineering, Colorado School of Mines,*
Colorado, United States of America

A good glass former, Ti$_{57.4}$Cu$_{33.4}$Ni$_{9.2}$, was selected using the topological instability criterion (lambda criterion) and the average electronegativity approach. The crystallization behavior and microstructural development of amorphous melt-spun ribbons of this new composition in response to heat treatment were investigated using a combination of differential scanning calorimetry (DSC), transmission electron microscopy (TEM) and X-ray diffraction (XRD). The results indicate that the crystallization of the Ti$_{57.4}$Cu$_{33.4}$Ni$_{9.2}$ alloy takes place through of three exothermic reactions with the nucleation of TiCu, Ti$_2$Cu and Ti$_2$Ni. The kinetics of crystallization were investigated by DSC, and the kinetic parameters were determined using Kissinger's method.

Keywords: *metallic glass, rapid-solidification, Kissinger method, ternary alloy systems*

1. Introduction

Amorphous alloys or metallic glasses are a relatively new class of materials with a specific combination of technologically interesting properties. These materials are characterized by the absence of formation of a regular crystal structure, and thus have a structural configuration similar to that of frozen liquid, where the process of nucleation and growth of a crystalline phase have been kinetically supplanted[1,2]. This structural configuration provides some properties that are frequently superior to those of crystalline materials, e.g., higher mechanical strength, improved magnetic, and/or electrical properties, and increased corrosion resistance.

The amorphous or glassy state is thermodynamically unstable and is structurally susceptible to devitrification when heated above the crystallization temperature (T$_x$), or when subjected to prolonged isothermal treatments below T$_x$. The process of devitrification of certain alloys can be controlled to favor the formation of a nanocrystalline structure or to obtain only a small fraction of crystallized material, with nanoparticles precipitated and incorporated into the residual amorphous phase. Various alloys that have such nanostructures or nanocrystals embedded in the matrix of an amorphous microstructure show better mechanical properties than those of alloys in the pure amorphous state. Thus, studies of controlled devitrification have attracted much interest in various research areas including physics, chemistry and materials science[3].

Such improved properties that are dependent on the microstructure have been studied exhaustively based on knowledge of the kinetics of crystallization of amorphous alloys allied to techniques such as microscopy and X-ray diffraction (DRX) analysis. Kinetic analyses can be performed using thermal analysis techniques such as isothermal or non-isothermal Differential Scanning Calorimetry (DSC)[4].

Considering the importance of both thermal stability and microstructural evolution during controlled devitrification on the resulting properties of amorphous alloys, the purpose of this work was to characterize the crystallization of the amorphous Ti$_{57.4}$Cu$_{33.4}$Ni$_{9.2}$ alloy from the kinetic standpoint and based on a structural analysis by DSC, DRX and by transmission electron microscopy (TEM). The kinetic analysis was performed using the Kissinger method[5].

The Ti-based bulk metallic glasses offer a combination of high specific strength, low density and relative low cost as well as other advantages of BMGs[6-8]. Ti-based metallic glasses presented yield stresses of up to 2200 MPa, which are much higher than the corresponding values for typical commercial Ti-based alloys in the range of 1000 MPa[9]. The good glass former Ti$_{57.4}$Cu$_{33.4}$Ni$_{9.2}$ was selected based on two distinct criteria: (i) the minimum topological instability criterion (λ-criterion) and (ii) the average difference in the alloy's electronegativity, and assuming a synergistic effect between them[10-13]. The topological instability parameter (λ) can be calculated from atomic radii or molar volumes of the compounds with the expression[12]:

$$\lambda \cong \sum \chi_i \left| \frac{Vm_i}{Vm_0} - 1 \right| \tag{1}$$

where χ_i is the molar fraction of any component element in a given stoichiometric compound (or simple metal), Vm_i is the molar volume of the solute elements and Vm_0 is the molar volume of the compound. On the other side, the average in electronegativity among the elements of an alloy is directly related to its formation enthalpy (ΔH) and its glass stability[5].

2. Experimental Procedures

A Ti$_{57.4}$Cu$_{33.4}$Ni$_{9.2}$ ingot was prepared by non-consumable arc melting of mixtures of pure Ti (99.97 wt.%), Ni (99.9 wt.%) and Cu (99.997 wt.%) in a Ti-gettered, high-purity argon atmosphere. The alloy was remelted under a high purity argon atmosphere in a quartz tube and injected through a nozzle onto a Cu wheel (200 mm diameter) rotating at a peripheral velocity of 30 ms^{-1} to produce rapidly-solidified ribbons by melt-spinning. The ribbons, with a width of ~ 2 mm and a thickness of about 20 microns, exhibited qualitatively a bending ductility of 180° and were characterized by X-ray diffraction (XRD) using Cu-K$_\alpha$ radiation (Philips X-Pert) and by transmission electron microscopy (Philips CM12 TEM with EDAX EDS). The crystallization process was evaluated using DSC (Netzsch 200 Maya F3) at heating rates of 5, 10, 20 and 40 K/min under an argon gas flow. To investigate the structural transformations by X-ray diffraction and by TEM, the melt-spun ribbons were heated from room temperature to different temperatures according to the DSC result (683, 713, 748, 788 K, 833 K and 973 K) in a DSC (without isothermal holding periods). The TEM specimens were prepared by twin-jet electropolishing in a solution of 66% methanol and 33% nitric acid at 243 K (25 V and 50 mA) and by argon ion milling in a Gatan dual ion mill (~1 mA and 6 kV).

3. Results and Discussion

Figure 1 presents the DSC thermogram of the alloy, indicating the temperature at which each heat treatment was performed. This figure depicts a three-stage devitrification process. Figure 2 shows the X-ray diffractograms after each heat treatment. It can be seen that the crystallization of the amorphous alloy was observed above 748 K with simultaneous precipitation of TiCu, Ti$_2$Cu and Ti$_2$Ni. However, in view of the large energy released in the third exothermic peak of the DSC thermogram, the amount of residual amorphous phase at this temperature of 748 K is still large. The melt-spun ribbons are fully crystallized above 833 K and contain the same TiCu, Ti$_2$Cu and Ti$_2$Ni phases.

From the XRD patterns exhibited in Figure 2, the first and second heat treatments (T$_1$ = 683 K and T$_2$ = 713 K) present a diffused peak characteristic of amorphous structures. In the third treatment (T$_3$ = 748 K) it is observed the formation of the TiCu, Ti$_2$Cu and Ti$_2$Ni phases, which probably were nucleated in the first exothermic reaction (peak 1 of the thermogram) and were not detected in the X-ray diffraction analysis due to its reduced size. However, this heat treatment at 748 K was performed near of the second exothermic peak, which may have provided sufficient energy for the growth
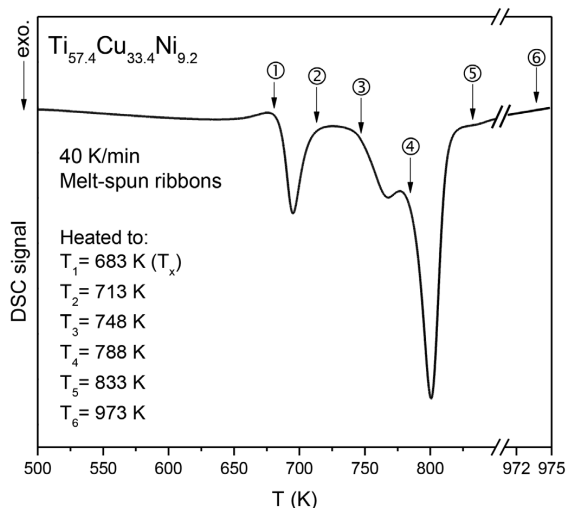
Figure 1. DSC thermogram of the ribbon, indicating the temperatures selected for the heat treatments.

of these nucleated phases. Finally, in the last heat treatment (T$_6$ = 973 K), in which the amorphous alloy was completely crystallized, it is observed the presence of the same phases: Ti$_2$Cu (I4/mmm), TiCu (P4/nmm) and Ti$_2$Ni (Fd3m).

Figure 3 shows the bright-field TEM micrographs and the corresponding SAPDs of the crystallization process. In (a) it is shown the micrographs of the second heat treatment, revealing an amorphous structure, in accordance with the X-ray analysis. In the next heat treatment shown in Figure 3b (T$_3$ = 748 K), it is observed the presence of a nanocrystalline structure with grains larger than the previously heat treated sample; besides, the selected area diffraction pattern (SADP) shows rings pattern characteristic of an nanocrystalline material. The fourth heat treatment (T$_4$ = 788 K) is exhibited in Figure 3c1 and c2, where it is observed larger grains and more well-defined rings patterns in the SADP, which were identified as Ti$_2$Cu, Ti$_2$Ni and TiCu, in accordance with the X-ray analysis. Figure 3c1 also shows the same morphological characteristics of Guinier-Preston (GP) zones (indicated by arrows) previously reported by Ishida & Sato[14] for compositions of the Ti$_{51.5}$Ni$_{48.5-x}$Cu$_x$ (x = 0-15.4) system; however, more studies are needed to confirm this observation in the present work. Figure 3d shows the micrograph of the sample heated to 833 K, where it is observed larger grains (~45 nm) and it is also possible to verify the rings pattern in the SADP with the same characteristic of the previously sample (Figure 3c2), indicating the presence of the same crystallized phases (Ti$_2$Cu, Ti$_2$Ni and TiCu). Finally, Figure 3e shows the sample heated to 973 K, approximately 150 K above the last crystallization peak, and the structure consisted of the same three phases previously crystallized.

To identify the early crystallized phases in the first exothermic peak, a heat treatment at 680 K for 1 hour was performed using a DSC. Figure 4a shows the bright-field TEM micrographs of the isothermal heat treated sample, where it is observed a eutectic-like lamellar microstructure in some grains of size of about 30 to 100 nm (indicated by arrow). This structure is consistent with the concomitant nucleation of the three phases observed in XRD and DSC analysis;
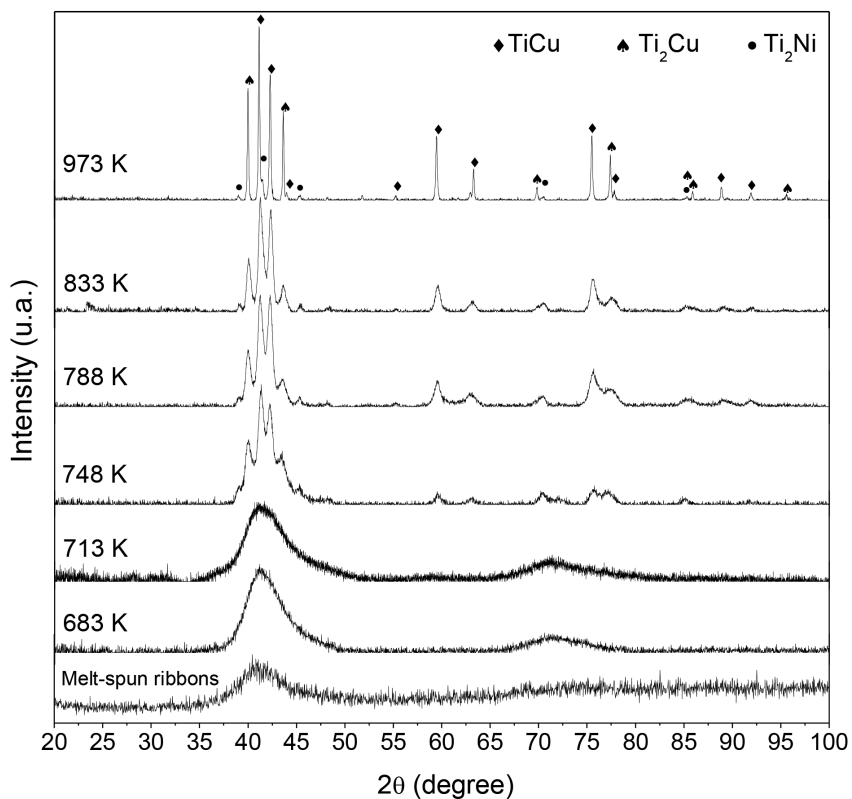
Figure 2. Diffractogram of the ribbon heated to: 683, 713, 748, 833 and 973 K.
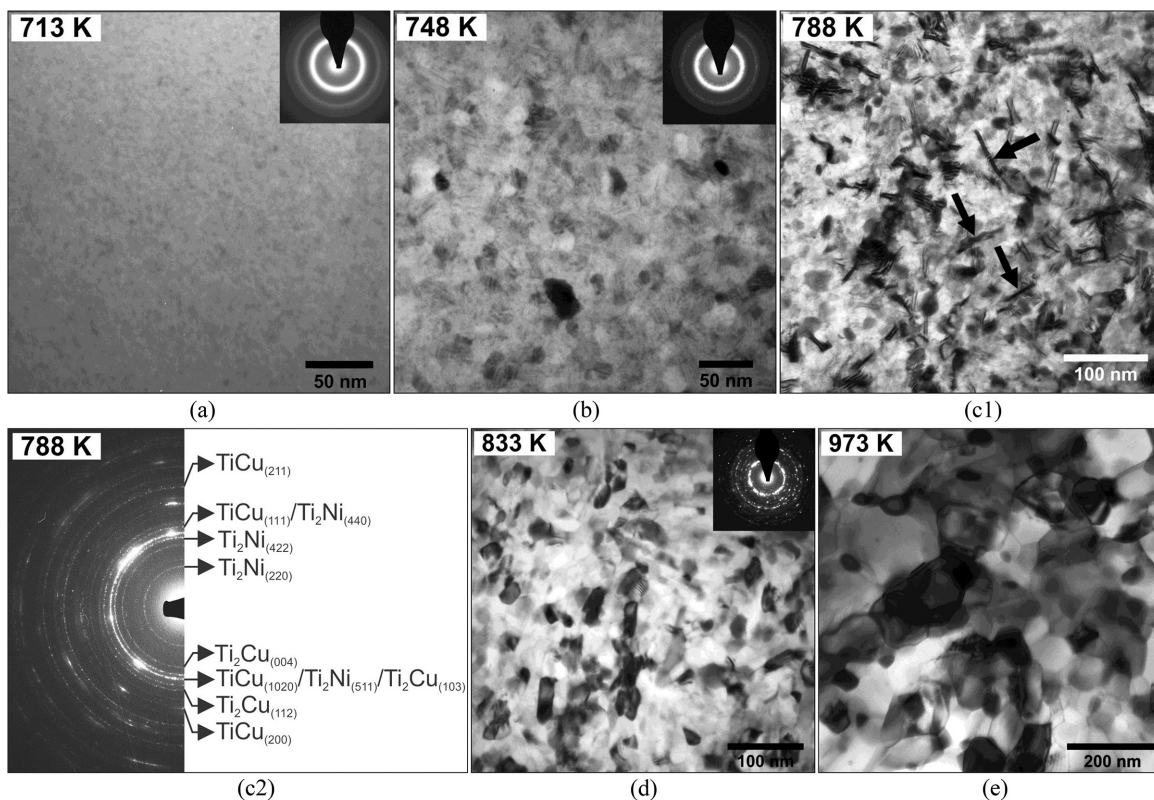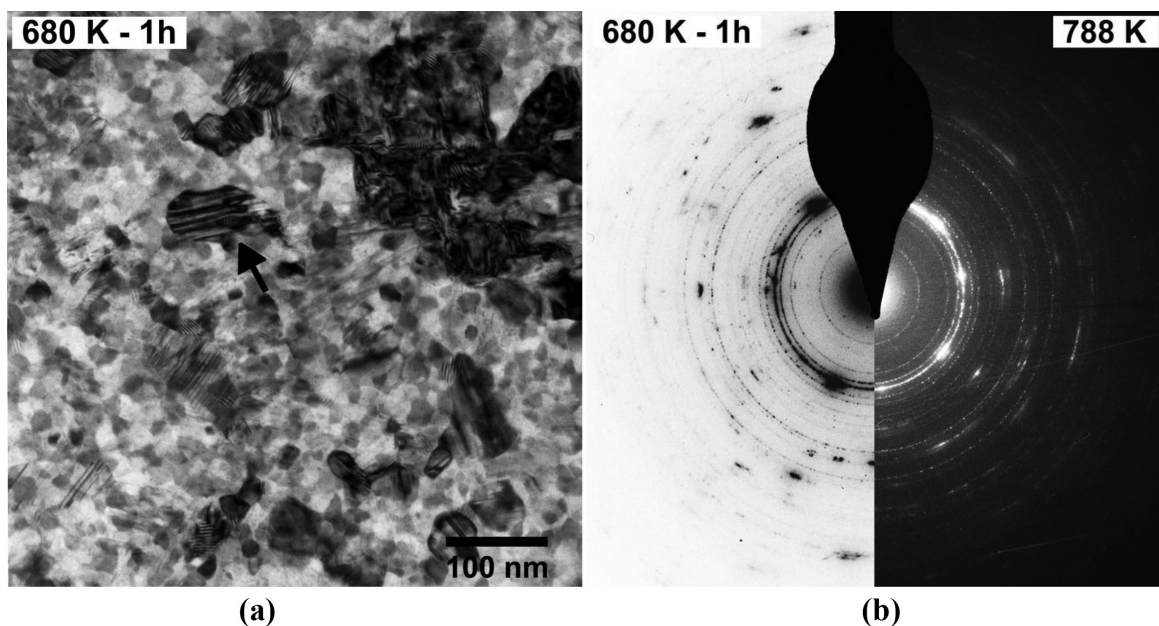

Figure 3. Bright-field TEM micrographs and corresponding SADPs of the ribbon heated to (a) 713 K; (b) 748 K; (c1, c2) 788 K; (d) 833 K; and (e) 973 K.

however, further analysis is required for confirming this type of devitrification. Figure 4b exhibits the microdiffraction patterns of the region and, in order to compare, it is also shown the microdiffraction patterns of the sample heated to 788 K (see Figure 3c2), revealing the presence of the same phases in both heat-treated samples.

The DSC thermograms and thermal parameters of the crystallization process of the Ti$_{51.1}$Cu$_{38.9}$Ni$_{10.0}$ glass obtained at different heating rates are shown in Figure 5a and

Table 1, respectively. Upon heating, the melt-spun ribbons exhibited three exothermic crystallization peaks as well as an endothermic reaction of structural relaxation, which characterizes the glass transition temperature (T$_g$). The glass transition temperature and both exothermic peaks shift to higher values with increasing heating rates, indicating the presence of kinetic effects. Figure 5b illustrates the result of applying the Kissinger method to each exothermic peak, where it is shown that the activation energy E_A of the two

Figure 4. (a) Bright-field TEM micrographs and (b) corresponding SADPs of the melt-spun ribbons heat treated at 680 K for 1 h. For comparison, it is also shown in (b) the SADPs of the sample heated to 788 K.
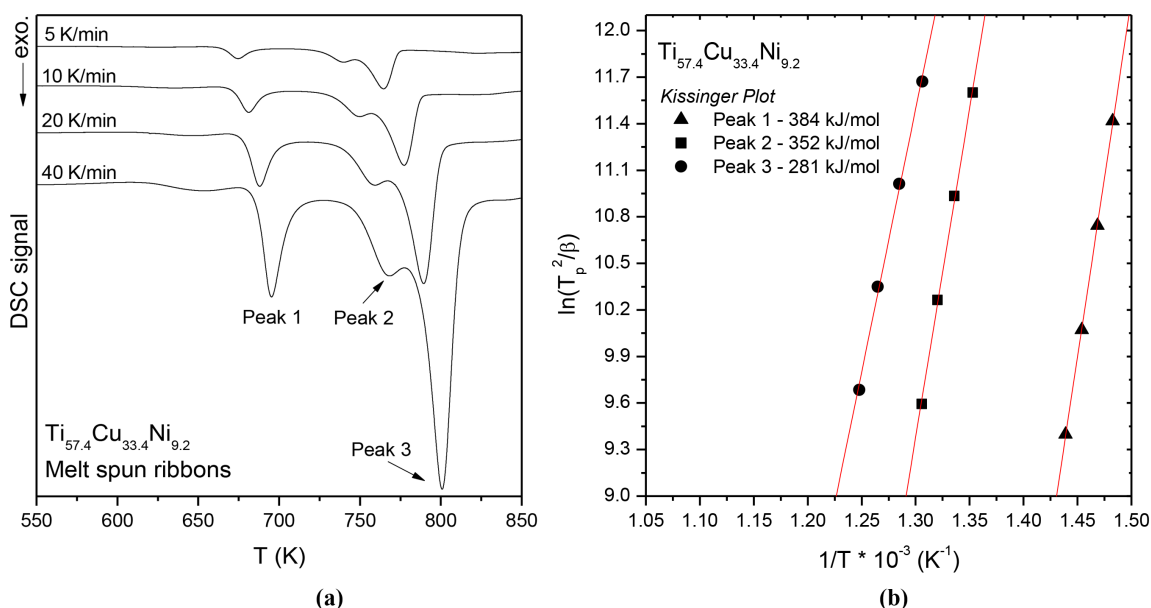
Figure 5. (a) DSC thermogram of the as-quenched ribbon at continuous heating rates of 5, 10, 20 and 40 K/min; (b) Kissinger plot of ln(Tp²/β) vs 1/T.

Table 1. Thermal parameters[a] obtained from the thermal analyses.

β (K/min)	T_g (K)	T_x (K)	T_1 (K)	T_2 (K)	T_3 (K)	H_1 (J/g)	H_2^b (J/g)
5	627.1	664.2	674.4	739.0	765.5	−18.5	−98.6
10	635.9	671.0	680.9	748.5	778.3	−20.1	−102.3
20	646.4	677.8	687.7	757.3	790.6	−21.3	−103.0
40	650.9	685.6	694.9	765.8	801.3	−23.5	−106.4

[a]Glass transition temperature (T_g); Crystallization onset temperature (T_x); temperatures at the exothermic peaks (T_1 and T_2); transformation enthalpies (H_1 and H_2); heating rate (β). [b]Total of second and third exothermic peaks.

first reactions is roughly the same, indicating that a similar nucleation and growth process occurs in the first and second exothermic reactions, whereas a dominant growth process occurs in the third reaction. These activation energy values are in agreement with previous reports in literature[15,16].

4. Conclusions

The results indicate that the crystallization of the $Ti_{57.4}Cu_{33.4}Ni_{9.2}$ alloy takes place through of three exothermic reactions with the nucleation of TiCu, Ti_2Cu and Ti_2Ni, occurring during the stages of crystallization. In the first stage of crystallization, it occurs with a high nucleation rate, resulting in a nanoscale microstructure. On the other hand, the heat-treated sample at 680 K for 1 h, before the crystallization temperature (T_x), suggests a eutectic-like lamellar structure with the presence of the TiCu, Ti_2Cu and Ti_2Ni phases. The results also indicate that a similar nucleation and growth process occurs in the first and second exothermic reactions, whereas a dominant growth process occurs in the third reaction.

Acknowledgements

References

1. Wang WH, Dong C and Shek CH. Bulk metallic glasses. *Materials Science and Engineering R Reports*. 2004; 44(2-3):45-89. http://dx.doi.org/10.1016/j.mser.2004.03.001.

2. Klement K, Willens RW and Duwez P. Non-crystalline structure in solidified gold-silicon alloys. *Nature*. 1960; 187(4740):869-870. http://dx.doi.org/10.1038/187869b0.

3. Louzguine-Luzgin DV and Inoue A. Nano-devitrification of glassy alloys. *Journal of Nanoscience and Nanotechnology*. 2005; 5(7):999-1014. http://dx.doi.org/10.1166/jnn.2005.158. PMid:16108420.

4. Starink MJ. Analysis of aluminium based alloys by calorimetry: quantitative analysis of reactions and reaction kinetics. *International Materials Reviews*. 2004; 49(3–4):191-226. http://dx.doi.org/10.1179/095066004225010532.

5. Kissinger HE. Reaction kinetics differential thermal analysis. *Analytical Chemistry*. 1957; 29(11):1702-1706. http://dx.doi.org/10.1021/ac60131a045.

6. Ma C, Ishihara S, Soejima H, Nishiyama N and Inoue A. Formation of new Ti-based metallic glassy alloys. *Materials Transactions*. 2004; 45(5):1802-1806. http://dx.doi.org/10.2320/matertrans.45.1802.

7. Sheng WB. Correlations between critical section thickness and glass-forming ability criteria of Ti-based bulk amorphous alloys. *Journal of Non-Crystalline Solids*. 2005; 351(37-39):3081-3086. http://dx.doi.org/10.1016/j.jnoncrysol.2005.07.021.

8. Gargarella P, Pauly S, Song KK, Hu J, Barekar NS, Khoshkhoo MS, et al. Ti-Cu-Ni shape memory bulk metallic glass composites. *Acta Materialia*. 2012; 61(1):151-162. http://dx.doi.org/10.1016/j.actamat.2012.09.042.

9. Oliveira MF, Pereira FS, Ramasco BT, Kiminami CS, Botta WJ and Bolfarini C. Glass formation of alloys selected by lambda and electronegativity criteria in the Ti–Zr–Fe–Co system. *Journal of Alloys and Compounds*. 2010; 495(2):316-318. http://dx.doi.org/10.1016/j.jallcom.2009.10.255.

10. Sá Lisboa RD, Bolfarini C, Botta WJF and Kiminami CS. Topological instability as a criterion for design and selection of aluminum-based glass-former alloys. *Applied Physics Letters*. 2005; 86(21):211904. http://dx.doi.org/10.1063/1.1931047.

11. Kiminami CS, Sá Lisboa RD, Oliveira MF, Bolfarini C and Botta WJ. Topological instability as a criterion for design and selection of easy glass-former compositions in Cu-Zr based systems. *Materials Transactions*. 2007; 48(7):1739-1742. http://dx.doi.org/10.2320/matertrans.MJ200745.

12. Oliveira MF, Pereira FS, Bolfarini C, Kiminami CS and Botta WJ. Topological instability, average electronegativity difference and glass forming ability of amorphous alloys. *Intermetallics*. 2009; 17(4):183-185. http://dx.doi.org/10.1016/j.intermet.2008.09.013.

13. Botta WJ, Pereira FS, Bolfarini C, Kiminami CS and Oliveira MF. Topological instability and electronegativity effects on the glass-forming ability of metallic alloys. *Philosophical Magazine Letters*. 2008; 88(11):785-791. http://dx.doi.org/10.1080/09500830802375622.

14. Ishida A and Sato M. Microstructures of crystallized $Ti_{51.5}Ni_{48.5-x}Cux$ ($x = 23.4$–37.3) thin films. *Intermetallics*. 2011; 19(7):900-907. http://dx.doi.org/10.1016/j.intermet.2011.02.005.

15. Yang YJ, Xing DW, Shen J, Sun JF, Wei SD, He HJ, et al. Crystallization kinetics of a bulk amorphous Cu–Ti–Zr–Ni alloy investigated by differential scanning calorimetry. *Journal of Alloys and Compounds*. 2006; 415(1-2):106-110. http://dx.doi.org/10.1016/j.jallcom.2005.07.062.

16. Patel AT and Pratap A. Kinetics of crystallization of $Zr_{52}Cu_{18}Ni_{14}Al_{10}Ti_6$ metallic glass. *Journal of Thermal Analysis and Calorimetry*. 2012; 107(1):159-165. http://dx.doi.org/10.1007/s10973-011-1549-y.